*J. Fluid Mech.* (1984), *vol.* 139, *pp.* 309–324
*Printed in Great Britain*



# Liquid-metal flow in a rectangular duct with a strong non-uniform magnetic field

By JOHN C. PETRYKOWSKI† AND JOHN S. WALKER
Department of Theoretical and Applied Mechanics, University of Illinois, Urbana, IL 61801

(Received 1 February 1983 and in revised form 4 October 1983)

Liquid-metal flows in rectangular ducts having electrically insulating tops and bottoms and perfectly conducting sides and in the presence of strong, polar, transverse magnetic fields are examined. Solutions are presented for the boundary layers adjacent to the sides that are parallel to the magnetic field. Overshoots in the radial velocity profiles show that the side layers have zero displacement thickness and do not perturb the inviscid core. Very weak secondary flows involve four significant vortices, as reflected in the polar velocity profiles.

## 1. Introduction

Fully developed MHD duct flows and three-dimensional MHD flows in variable-area ducts with strong uniform magnetic fields have received considerable attention (reviewed respectively by Hunt & Shercliff (1971) and by Walker & Ludford (1975)), but three-dimensional MHD duct flows in strong non-uniform magnetic fields are less well understood. For large, direct-current, electromagnetic feed pumps in liquid-metal fast-breeder reactors and for liquid-lithium blankets in magnetic-confinement fusion reactors, the flows in regions of strong non-uniform magnetic fields are major contributors to the pressure drops and energy losses.

MHD flows in circular ducts with strong non-uniform magnetic fields have been studied analytically by Holroyd & Walker (1978) and experimentally by Holroyd (1979, 1980*b*). Inviscid flows in rectangular ducts having insulating tops and bottoms and highly conducting sides and in the presence of planar non-uniform magnetic fields which are parallel to the sides have been studied analytically and experimentally by Holroyd (1980*a*). Here we extend Holroyd's analysis to include viscous effects in the boundary layers, while restricting the geometry and magnetic field in order to make the side-layer boundary-value problems tractable.

The Hartmann layers adjacent to the top and bottom have a well-known, local exponential structure, but the side-layer solutions for various cases are much more difficult than the corresponding solutions with uniform magnetic fields. Ludford & Walker (1980) formulate these side-layer governing equations for non-uniform, planar magnetic fields for various wall conductivities, but they do not present any solutions. They point out that these equations can be solved locally only for perfectly conducting sides and that the coefficients in the governing partial differential equations are constants only for polar magnetic fields. Therefore the present study treats the simplest possible non-uniform magnetic field, side-layer problem.

The results apply to the flows near the ends of the electrodes and magnet pole faces of the LMFBR feed pump, but do not apply to the flows beyond the electrode ends

† Present address: Oak Ridge National Laboratory, Oak Ridge, Tennessee 37830.

or to fusion blanket flows, since these cases involve thin metal sides rather than perfectly conducting sides. However, insights from the present simplest possible case and empirically derived simplifications (Holroyd 1980*a*) can be used in the future to make the more difficult side-layer problems for thin conducting or insulating sides and for non-polar magnetic fields tractable.

## 2. Problem formulation and core solution

The dimensionless equations governing the steady flow of an electrically conducting, incompressible fluid in the presence of a steady magnetic field are

$$N^{-1}(\boldsymbol{v}\cdot\nabla)\,\boldsymbol{v} = -\nabla p + \boldsymbol{j}\times\boldsymbol{B} + M^{-2}\nabla^2\boldsymbol{v}, \tag{1a}$$

$$\boldsymbol{j} = -\nabla\phi + \boldsymbol{v}\times\boldsymbol{B}, \quad \nabla\cdot\boldsymbol{j} = 0, \tag{1b, c}$$

$$\nabla\cdot\boldsymbol{v} = 0, \quad \nabla\cdot\boldsymbol{B} = 0, \quad \nabla\times\boldsymbol{B} = R_{\mathrm{m}}\boldsymbol{j}, \tag{1d, e, f}$$

where $\boldsymbol{v}$, $p$, $\boldsymbol{j}$, $\boldsymbol{B}$ and $\phi$ are the velocity, pressure, electric current density, magnetic field and electric potential function, which are normalized using $V_0$, $\sigma V_0 B_0^2 L$, $\sigma V_0 B_0$, $B_0$ and $V_0 B_0 L$ respectively (Walker 1980). The dimensionless parameters

$$N = \sigma B_0^2 \frac{L}{\rho V_0}, \quad M = B_0 L\left(\frac{\sigma}{\eta}\right)^{\frac{1}{2}}, \quad R_{\mathrm{m}} = \mu\sigma V_0 L$$

are the interaction parameter. Hartmann number and magnetic Reynolds number; $L$, $V_0$ and $B_0$ are the characteristic length, velocity and magnetic field strength for a particular flow situation; and $\sigma$, $\rho$, $\eta$ and $\mu$ are the fluid's electrical conductivity, density, dynamic viscosity and magnetic permeability, which are assumed to be constant.

We assume (i) that $R_{\mathrm{m}} \ll 1$, so that $\boldsymbol{B}$ in (1*a*, *b*) is a known vector field given by solving the decoupled equations (1*e*, *f*) with zero on the right-hand side of (1*f*), and (ii) that $N \gg M \gg 1$, so that the inertial term on the left-hand side of (1*a*) is negligible everywhere (Walker, Ludford & Hunt 1971), and so that viscous effects are confined to boundary and free shear layers. The dimensionless polar magnetic field has the components

$$B_r = B_z = 0, \quad B_\theta = r^{-1}, \tag{2}$$

where $(r, \theta, z)$ are cylindrical coordinates, and $B_0$ is chosen as the magnetic field strength at a distance $L$ from the $z$-axis. The duct has straight, diverging, electrically insulating top and bottom, which are perpendicular to the magnetic field at $\theta = \pm\theta_0$ and parallel, perfectly conducting sides which are parallel to the magnetic field at $z = \pm 1$, where $L$ is chosen as half the distance between the sides (see figure 1).

In addition to satisfying a modified form of (1*a–d*) with the left-hand side of (1*a*) replaced by zero, with the components of $\boldsymbol{B}$ given by (2) and with $M \gg 1$, the variables $\boldsymbol{v}$, $p$, $\boldsymbol{j}$ and $\phi$ must satisfy the boundary conditions

$$\boldsymbol{v} = 0, \quad j_\theta = 0 \quad \text{at} \quad \theta = \pm\theta_0, \tag{3a, b}$$

$$\boldsymbol{v} = 0, \quad \phi = \pm\phi_0 \quad \text{at} \quad z = \pm 1. \tag{4a, b}$$

The boundary condition (3*b*) assumes that $c_{\mathrm{t,\,b}} \ll M^{-1}$, while the boundary condition (4*b*) assumes that $c_{\mathrm{s}} \gg M^{\frac{1}{2}}$, where $c_i = \sigma_i t_i/\sigma L$ is the wall conductance ratio for the wall with electrical conductivity $\sigma_i$ and thickness $t_i$, and $i$ = t, b and s for the top, bottom and sides respectively (Walker 1981).

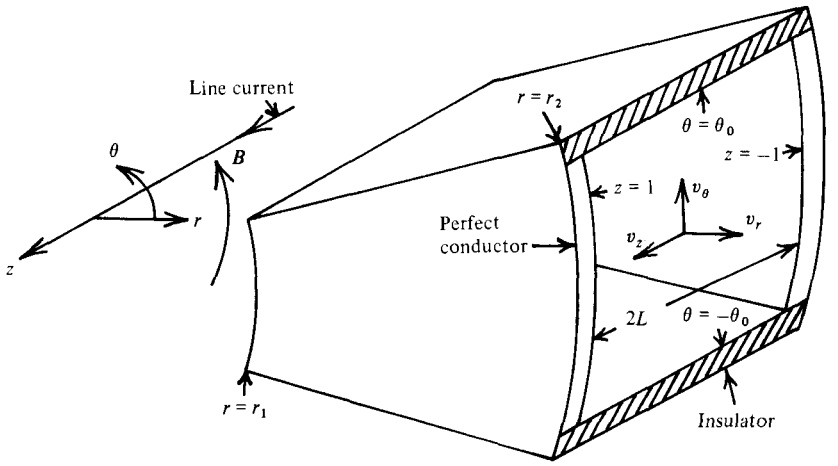


FIGURE 1. The duct with the cylindrical coordinates, the components of velocity, and an infinite line current along the $z$-axis which would produce the present polar magnetic field.

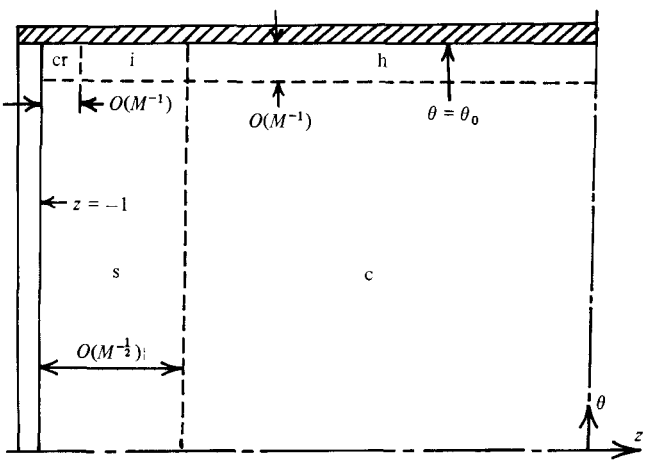


FIGURE 2. One quarter ($0 \leqslant \theta \leqslant \theta_0$, $-1 \leqslant z \leqslant 0$) of an $r$ = constant cross-section of the duct showing the subregions of the flow for $M \gg 1$.

The average velocity at a distance $L$ from the $z$-axis is chosen as $V_0$, so that the dimensionless radial velocity must satisfy a volume-flux condition

$$\int_{-1}^{1}\int_{-\theta_0}^{\theta_0} v_r r \,\mathrm{d}\theta\,\mathrm{d}z = 4\theta_0. \tag{5}$$

The modified equations (1*a–d*) and the boundary conditions (3, 4) represent a linear boundary-value problem whose homogeneous solution is normalized by the volume-flux condition (5).

The interior of the duct can be divided into subregions, and certain terms in the modified equations (1*a–d*) can be neglected in each subregion. The subregions (shown in figure 2) are (c) the inviscid core, (h) the Hartmann layers with $O(M^{-1})$ thickness, (s) the side layers with $O(M^{-\frac{1}{2}})$ thickness, (i) the intersection regions with $O(M^{-1}) \times O(M^{-\frac{1}{2}})$ dimensions, and (cr) the corner regions with $O(M^{-1}) \times O(M^{-1})$ dimensions. The corner regions are needed to represent singularities properly in the

side-layer solution at the corners, but we can obtain the first term in each asymptotic expansion for the variables in the other subregions without considering the corner regions in detail.

All derivatives are $O(1)$ in the core, so that the core variables satisfy the modified equations (1*a–d*) neglecting the last, $O(M^{-2})$, viscous term in (1*a*). The Hartmann layers have a well-known exponential structure which depends only on the local, tangential core velocity. The Hartmann-layer variables satisfy the boundary conditions (3) and match the core variables, provided the latter satisfy the Hartmann conditions

$$v_\theta = j_\theta = 0 \quad \text{at} \quad \theta = \pm\theta_0, \tag{6}$$

neglecting $O(M^{-1})$ terms (Walker, Ludford & Hunt 1972). In the side layers $v_r$ and $v_\theta$ are $O(1)$, and the jumps in $v_z$ and $\phi$ across the side layers are at most $O(M^{-\frac{1}{2}})$. Therefore the boundary conditions (4) indicate that the core variables satisfy the conditions

$$v_z = 0, \quad \phi = \pm\phi_0 \quad \text{at} \quad z = \pm 1, \tag{7}$$

neglecting $O(M^{-\frac{1}{2}})$ terms. The core variables which satisfy the inviscid governing equations, the boundary conditions (6, 7) and the volume-flux condition (5) are

$$\left.\begin{aligned} &v_r = r^{-1}, \quad v_\theta = v_z = j_r = j_\theta = 0, \quad j_z = r^{-2} - \phi_0, \\ &\phi = \phi_0 z, \quad p = \phi_0 \ln r + \frac{1}{2r^2}, \end{aligned}\right\} \tag{8}$$

where $O(M^{-\frac{1}{2}})$ terms are neglected, and inessential additive constants in the pressure and electric potential have been set equal to zero. The solution (8) can be obtained by substituting the present magnetic field (2) into the general inviscid solution presented by Holroyd (1980*a*).

In the analysis of the side layers we will need some of the $O(M^{-\frac{1}{2}})$ and $O(M^{-1})$ core perturbation variables, while these variables satisfy the same inviscid version of the modified equations (1*a–d*), which neglects $O(M^{-2})$ terms. In addition, the $O(M^{-\frac{1}{2}})$ core perturbation variables also satisfy the Hartmann conditions (6), which neglect $O(M^{-1})$ terms. With these requirements, the $O(M^{-1})$ core perturbation pressure is a function of $r$ and $z$ only, while the $O(M^{-\frac{1}{2}})$ core perturbation pressure $h$ is a function of $r$ only, and the $O(M^{-\frac{1}{2}})$ core perturbation electric potential function is given by

$$\frac{z}{2r}(r^3 h')', \tag{9}$$

where the primes denote differentiation with respect to $r$, and another inessential, additive, constant voltage has been discarded.

If the perfectly conducting sides are connected to an external d.c. voltage source, then $\phi_0$ equals half the dimensionless voltage difference. On the other hand, if the sides from an entrance at $r = r_1$ to an exit at $r = r_2$ are connected to an external resistor, then

$$\phi_0 = \frac{2\ln(r_2/r_1)}{r_2^2 - r_1^2 + 2/R\theta_0},$$

where $R$ is the dimensionless external resistance normalized with respect to $1/\sigma L$. The value of $\phi_0$ increases from zero for a short circuit ($R = 0$) to a maximum for an open circuit ($R = \infty$). For an open circuit there is no net $O(1)$ transverse electric current, but the $O(1)$ transverse electric current density $j_z$ is positive from $r = r_1$ to

$$r = \left[\frac{r_2^2 - r_1^2}{2\ln(r_2/r_1)}\right]^{\frac{1}{2}},$$

and is negative from this radius to $r = r_2$. Correspondingly the pressure decreases from its value at the entrance to a minimum at this radius, and then increases to an exit pressure which is less than the entrance pressure. The pressure measurements presented by Holroyd (1980*a*) are qualitatively similar.

The core solution (8) and the side-layer solution to be presented in §3 are independent of any boundary conditions at $r = r_1, r_2$. In other words, the solutions in the present finite-length duct are the same regardless of the flows upstream and downstream of its entrance and exit, respectively. If the upstream and downstream flows do not exactly match the core and side-layer solutions, then free shear layers of $O(M^{-\frac{1}{2}})$ thickness at $r = r_1, r_2$ provide whatever adjustments are necessary (Ludford & Walker 1976).

## 3. Side-layer solution

The flow is symmetric in $z$, so that we need only consider the side layer at $z = -1$. The substitutions

$$z = -1 + \frac{rZ}{M^{\frac{1}{2}}}, \quad v_r = \frac{V_r}{r}, \quad v_\theta = \frac{V_\theta}{r}, \tag{10a, b, c}$$

$$v_z = \left[\frac{r}{2}\left(\frac{(r^3h')'}{r}\right)' + \frac{V_z}{r}\right] \Big/ M^{\frac{1}{2}}, \tag{10d}$$

$$j_r = \frac{J_r}{r^2 M^{\frac{1}{2}}}, \quad j_\theta = \frac{J_\theta}{r^2 M^{\frac{1}{2}}}, \tag{10e, f}$$

$$j_z = r^{-2} - \phi_0 - \frac{rh'}{M^{\frac{1}{2}}} + \frac{J_z - r^3 g'}{r^2 M}, \tag{10g}$$

$$\phi = -\phi_0 + \left[\phi_0 rZ - \frac{(r^3h')'}{2r} + \frac{\Phi}{r}\right] \Big/ M^{\frac{1}{2}}, \tag{10h}$$

$$p = \phi_0 \ln r + \tfrac{1}{2}r^2 + \frac{h}{M^{\frac{1}{2}}} + \left(g + \frac{P}{r^2}\right) \Big/ M \tag{10i}$$

stretch the coordinate normal to the side and introduce rescaled side-layer variables, which are denoted by capital letters and which are functions of the side-layer coordinates $(r, \theta, Z)$. Here $h$ is the $O(M^{-\frac{1}{2}})$ core perturbation pressure, which is a function of $r$ only, and $g$ is the $O(M^{-1})$ core perturbation pressure evaluated at $z = -1$, so that $g$ is also a function of $r$ only, while primes denote differentiation with respect to $r$. The additive terms in the substitutions (10*d*, *g–i*) come from the matching between the side-layer and core solutions, so that all side-layer variables except $V_r$ vanish as $Z \to \infty$, while $V_r \to 1$. The powers of $r$ rescaling each side-layer variable are chosen because these particular rescaled variables turn out to be independent of $r$. The variables (10*b–i*) now represent the leading terms in the asymptotic expansions for the side-layer variables, so that the expressions (10*b*, *c*) neglect $O(M^{-\frac{1}{2}})$ terms, the expressions (10*d–f*, *h*) neglect $O(M^{-1})$ terms, and the expressions (10*g*, *i*) neglect $O(M^{-\frac{3}{2}})$ terms.

With the substitutions (2), (10) and with some algebraic manipulations, the leading

terms in the inertialess version of the governing equations (1*a–d*) provide three equations,

$$\frac{\partial^2 \Phi}{\partial \theta^2} - \frac{\partial^4 \Phi}{\partial Z^4} = 2\frac{\partial P}{\partial Z}, \tag{11a}$$

$$\frac{\partial V_\theta}{\partial \theta} - \frac{\partial^2 P}{\partial Z^2} = -2\frac{\partial \Phi}{\partial Z}, \tag{11b}$$

$$\frac{\partial P}{\partial \theta} - \frac{\partial^2 V_\theta}{\partial Z^2} = 0, \tag{11c}$$

governing the three basic side-layer variables $\Phi$, $V_\theta$ and $P$, and also provide expressions for the other side-layer variables in terms of these three basic ones,

$$V_r = 1 + \frac{\partial \Phi}{\partial Z}, \quad V_z = S(\Phi) - \frac{\partial P}{\partial Z}, \tag{12a, b}$$

$$J_r = \frac{\partial P}{\partial Z}, \quad J_\theta = -\frac{\partial \Phi}{\partial \theta}, \tag{12c, d}$$

$$J_z = P + S(P) + \frac{\partial^3 \Phi}{\partial Z^3}, \tag{12e}$$

where

$$S(P) = P + Z\frac{\partial P}{\partial Z} - r\frac{\partial P}{\partial r}. \tag{13}$$

The terms on the right-hand sides of the equations (11*a*, *b*) represent the effects of this non-uniform magnetic field on the side layers. If the right-hand sides of (11*a*, *b*) were replaced by zeros, the equations (11) would become the three basic side-layer equations for a variable-area duct with a uniform, transverse magnetic field (Walker, Ludford & Hunt 1971). For a uniform magnetic field, the equation (11*a*) governing $\Phi$ is decoupled from the equations (11*b*, *c*) governing $P$ and $V_y$, the component of velocity parallel to the magnetic field; the boundary-value problems are only coupled through the the Hartman conditions at the top and bottom. For a non-uniform magnetic field, the three basic side-layer variables are intrinsically coupled because of the right-hand sides of the equations (11*a*, *b*).

With the substitution of the expressions (10*a–d*, *h*, 12*a*, *b*, 13), the boundary conditions (4) become

$$\left.\begin{aligned} \frac{\partial \Phi}{\partial Z} &= -1, \quad \frac{\partial P}{\partial Z} = 0, && (14a, b)\\ V_\theta &= 0, \quad \Phi = \tfrac{1}{2}(r^3 h')' && (14c, d) \end{aligned}\right\} \quad \text{at} \quad Z = 0.$$

Walker *et al.* (1972) treat the Hartmann layers and intersection regions on general insulators with uniform magnetic fields, while Holroyd & Walker (1978) extend this treatment to non-uniform magnetic fields. The intersection-region variables satisfy the boundary conditions (3) and match the side-layer variables (10), provided the latter satisfy the Hartmann conditions

$$V_\theta = 0, \quad J_\theta = \mp \frac{\partial V_r}{\partial Z}, \quad \text{at} \quad \theta = \pm\theta_0, \tag{15a, b}$$

which neglect $O(M^{-\frac{1}{2}})$ and $O(M^{-1})$ terms respectively. Substituting the expressions (12*a*, *d*), the boundary conditions (15*b*) become

$$\frac{\partial \Phi}{\partial \theta} = \pm \frac{\partial^2 \Phi}{\partial Z^2} \quad \text{at} \quad \theta = \pm \theta_0. \tag{16}$$

The matching between the core and side-layer solutions yields the conditions

$$\Phi \to 0, \quad V_\theta \to 0, \quad P \to 0 \quad \text{as} \quad Z \to \infty. \tag{17a, b, c}$$

The $O(M^{-\frac{1}{2}})$ core perturbation solution is determined by the structure of the side layer, which satisfies the boundary conditions (4) and matches the $O(1)$ core solution (8). If we integrate (11*b*) from $\theta = -\theta_0$ to $\theta = \theta_0$ and from $Z = 0$ to $Z = \infty$, and if we introduce the boundary conditions (14*b*, *d*, 15*a*, 17*a*, *c*), then we obtain the restriction

$$(r^3 h')' = 0,$$

so that $h' = C/r^3$, where $C$ is a constant of integration. The boundary condition (14*d*) is now replaced by

$$\Phi = 0 \quad \text{at} \quad Z = 0. \tag{18}$$

The equation (12*a*) and the boundary conditions (17*a*, 18) show that the side layers have no $O(M^{-\frac{1}{2}})$ volume-flux deficiency. Since the Hartmann-layer volume-flux deficiency is $O(M^{-1})$, the $O(M^{-\frac{1}{2}})$ core perturbation radial velocity, which is equal to $-C/r$, must satisfy the volume-flux condition (5) with the $4\theta_0$ on the right-hand side replaced by zero. Therefore $C = 0$, and all $O(M^{-\frac{1}{2}})$ core perturbation variables are zero, so that the core solution (8) actually neglects $O(M^{-1})$ terms.

The boundary-value problem (11, 14*a*–*c*, 15*a*, 16, 17, 18) is completely independent of $r$, so that the solutions $\Phi$, $V_\theta$ and $P$ are functions of $\theta$ and $Z$ only. The last term in the expression (13) is zero, and all the rescaled side-layer variables denoted by capital letters are functions of $\theta$ and $Z$ only. Indeed, the side-layer variables represent a one-parameter family of universal profile functions of $\theta$ and $Z$, which depend only on the parameter $\theta_0$.

The method used to solve the boundary-value problem (11, 14*a*–*c*, 15*a*, 16, 17, 18) represents an extension of the solution technique for the side layers in similar rectangular ducts with uniform, transverse magnetic fields (Walker *et al.* 1971). Here we will summarize the method, with emphasis on the new elements required for the non-uniform magnetic field side-layer problem. A Fourier sine transform with respect to $Z$ is introduced for $\Phi$, while Fourier cosine transforms are introduced for $P$ and $V_\theta$. These transforms reduce the equations (11) to one second-order and two first-order ordinary differential equations with $\theta$ as the independent variable. This particular combination of Fourier sine and cosine transforms incorporates the boundary conditions (14*b*, 17, 18) into the ordinary differential equations, ignores the boundary conditions (14*a*, *c*), and introduces an inhomogeneous term involving an unknown function of $\theta$ into the transforms of each of the equations (11*a*, *c*). The two unknown functions

$$F(\theta) = \frac{\partial^2 \Phi}{\partial Z^2} = \frac{\partial V_r}{\partial Z}, \quad G(\theta) = \frac{\partial V_\theta}{\partial Z} \quad \text{at} \quad Z = 0$$

are the rescaled dimensionless shear stresses $\tau_{rz}$ and $\tau_{\theta z}$ at the side. The solution of the three ordinary differential equations must satisfy the cosine and sine transforms of the boundary conditions (15*a*, 16) respectively at $\theta = \pm \theta_0$.

The solutions for the transforms of $\Phi$, $P$ and $V_\theta$ can be found in terms of $F$ and $G$ using either the method of variation of parameters or a Green-function approach,

and solutions were found by both methods as a check on the lengthy algebraic steps involved. For a uniform magnetic field, the equation governing $\Phi$ is decoupled from the equations governing $P$ and $V_y$, so that the Green-function solutions can be generated separately; the coupling through the Hartmann conditions can be taken care of by the homogeneous solutions. For this non-uniform magnetic field, the three ordinary differential equations are intrinsically coupled through the transforms of the right-hand sides of (11*a*, *b*), so that the Green-function and variation of parameter methods are being applied to a single fourth-order problem, rather than to two decoupled second-order problems.

Analytic Fourier inversions are not possible, so that the solution for $\Phi$ and the solutions for $P$ and $V_\theta$ are given by quadrature representations of these inversion integrals involving the sine and cosine respectively of $Z$ times the Fourier transform variable $\lambda$, with integration from $\lambda = 0$ to $\lambda = \infty$. After interchanging the order of integration, the solution for each of the variables $\Phi$, $P$ and $V_\theta$ is given by the sum of two integrals with respect to an integration variable $\theta^*$. The integrand of each integral consists of either $F(\theta^*)$ or $G(\theta^*)$ times a kernel which is a function of $\theta$, $\theta^*$ and $Z$, and which is given by a semi-infinite integral with respect to $\lambda$.

When we introduce the solutions for $\Phi$ and $V_\theta$ into the previously ignored boundary conditions (14*a*, *c*), we obtain a pair of coupled integral equations governing the unknown wall shear stresses $F$ and $G$. The integral equation generated by the condition (14*a*) involves an inhomogeneous term equal to $-1$, while the other integral equation is homogeneous. Each integral equation holds for $-\theta_0 \leqslant \theta \leqslant \theta_0$ and involves an integral from $\theta^* = -\theta_0$ to $\theta^* = \theta_0$ for each of the unknown functions. For each of the four integrals, $F(\theta^*)$ or $G(\theta^*)$ is multiplied by a kernal which is now a function of $\theta$ and $\theta^*$ only, and which is given by a semi-infinite integral with respect to $\lambda$.

For the corresponding uniform magnetic field side-layer problem, pairs of kernels are the same, so that the two integral equations can be simply summed to obtain one integral equation with one kernel and one unknown function, which is the sum of $F$ and $G$. Once the single unknown function is found, it is easily split into $F$ and $G$ because $F$ and $G$ are even and odd functions respectively (Walker *et al.* 1971). The coupling due to this non-uniform magnetic field eliminates this equality between kernels, so that we must deal with two integral equations, instead of one, and with four kernels instead of one. In addition, the kernels here involve extremely long and complex algebraic expressions. Each of the kernels for the uniform field problem can be presented in one line, while each of the present kernels requires three pages for presentation. Therefore the four kernels in the integral equations and the six kernels in the expressions for the basic side-layer variables are not presented here, but are presented by Petrykowski (1981).

The solution of the two coupled integral equations gives $F$ and $G$. Then the solutions for $\Phi$, $P$ and $V_\theta$ are obtained by introducing the solutions for $F$ and $G$ into the expressions obtained by the Fourier inversion of the Green-function solutions. The solutions for the other side-layer variables are obtained by introducing the solutions for the three basic variables into the expressions (12). Numerical analysis is required for all of these steps.

Thirty-two-point Gauss–Legendre, Gauss–Hermite and Gauss–Chebyshev quadratures are used to solve the integral equations for $F$ and $G$. The four integrals with respect to $\theta^*$ are approximated by the Gauss–Chebyshev quadrature because the kernels have square-root singularities at $\theta = \theta^* = \pm\theta_0$. Walker *et al.* (1971) used a Gauss–Legendre quadrature for similar integrals, but they had to rescale the variable

of integration because of the corresponding square-root singularities. Since a Gauss quadrature based on Chebyshev polynomials of the first kind automatically provides the concentration of abscissas near the end points which is appropriate for square-root singularities, the Gauss–Chebyshev quadrature requires no rescaling and involves a smaller, bounded remainder, so the use of this quadrature represents an improvement over the previous numerical analysis.

The kernels behave like $|\theta-\theta^*|^{-\frac{1}{2}}$ near $\theta^* = \theta$, and two steps are needed to represent this singularity properly in the numerical approximation. First, integrals with $F(\theta^*)$ and $G(\theta^*)$ replaced by $F(\theta)$ and $G(\theta)$ are added to and subtracted from the corresponding integrals in the integral equations. For the added integrals, the $F$ or $G$ is taken out of each integral, so that the remaining integrand is known and analytically integrable. After integration, the only singularities are at $\theta = \pm\theta_0$ and present no problems. The subtracted integrals are incorporated into the original integrals, so that the combined integrands are zero at $\theta = \theta^*$ because the square-root singularity is multiplied by $F(\theta^*)-F(\theta)$ or $G(\theta^*)-G(\theta)$. While this first step removes the singularity at $\theta = \theta^*$, the contribution of the diagnonal $\theta = \theta^*$ is still very important in the integral equations. The second step is to evaluate both integral equations at values of $\theta$ which are equal to the 32 Gauss–Chebyshev abscissas. Use of the same discrete values for $\theta$ and $\theta^*$ properly represents the contribution of the diagonal, once the singularity here has been removed.

These steps reduce the pair of coupled integral equations to a matrix equation corresponding to 64 simultaneous, linear, algebraic equations. A $64 \times 64$ square matrix multiplies a $64 \times 1$ column matrix composed of the 32 unknown values of $F$ at the Gauss–Chebyshev abscissa values and the 32 unknown values of $G$ at the same abscissa values. The product of these matrices equals a known, $64 \times 1$ column matrix with 32 values of $-1$ and 32 values of 0. The 4096 values in the square matrix are the values of the four kernels in the integral equations evaluated at various values of $\theta$ and $\theta^*$, and multiplied by the Gauss–Chebyshev weight factors. For the numerical evaluation of the semi-infinite integrals with respect to $\lambda$ which define the four kernels, the 16 positive abscissas for the 32-point Gauss–Legendre quadrature are used for the part of each integral from $\lambda = 0$ to some fixed value of $\lambda$, and the 16 positive abscissas for the 32-point Gauss–Hermite quadrature are used for the part of each integral from this fixed value to $\lambda = \infty$. For the uniform magnetic field side-layer problem, Walker *et al.* (1971) split each of the integrands in their semi-infinite Fourier inversion integrals into two integrands: one integrand that could be integrated analytically with respect to $\lambda$ and one integrand that behaved like $\exp(-2\lambda^2)$ as $\lambda \to \infty$. With this splitting, the semi-infinite integrals requiring numerical evaluation had the exponential behaviour appropriate for a Gauss–Hermite quadrature. For the present non-uniform magnetic field side-layer problem, the integrals for the kernels are vastly more complicated than those for the uniform-field problem, and no splitting of the present integrals yields either analytically integrable parts or uniformly exponential behaviour. Instead, $\lambda$ in each semi-infinite integral must be rescaled by one of three functions of $\theta$ and $\theta^*$ in order to ensure the proper exponential behaviour of the integrand as the rescaled $\lambda$ approaches infinity. Various fixed values of $\lambda$ separating the integration ranges for the Gauss–Legendre and Gauss–Hermite quadratures were used in order to check the accuracy of the numerical approximations for the kernels.

After the 4096 values in the square matrix are obtained from the Gauss–Legendre and Gauss–Hermite approximations for the semi-infinite Fourier-inversion integrals, the values of $F$ and $G$ at the 32 Gauss–Chebyshev abscissas are found by Gauss

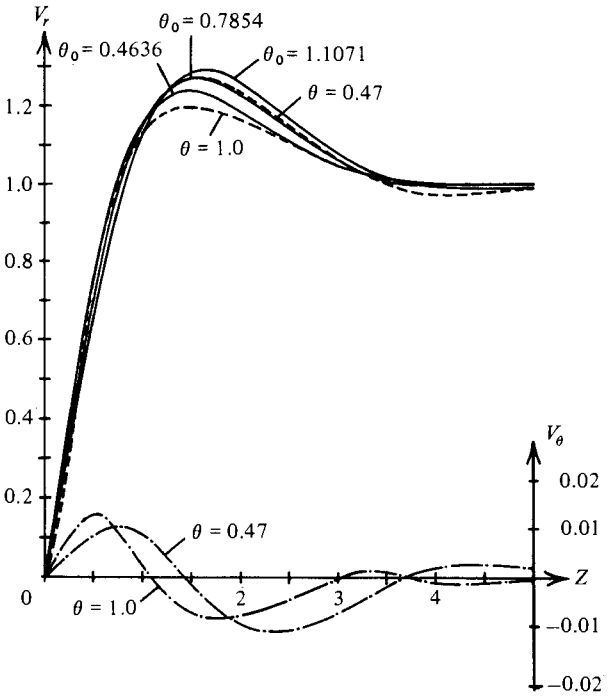


FIGURE 3. Profiles of the rescaled side-layer radial velocity $V_r$ and polar velocity $V_\theta$. Solid lines denote $V_r$ in the midplane ($\theta = 0$) for $\theta_0 = 0.4636$, 0.7854 and 1.1071 radians ($\tan\theta_0 = 0.5$, 1.0 and 2.0 respectively). Dashed lines denotes $V_r$ at other values of $\theta$ for $\theta_0 = 1.1071$ rad. Dot–dashed lines denote $V_\theta$ for $\theta_0 = 1.1071$ rad.

elimination with row pivoting. The solutions for $\Phi$, $P$ and $V_\theta$, as well as the solutions (12) for the other side-layer variables, are each given by the sum of two integrals with respect to $\theta^*$, where the integrands consist of $F$ or $G$ times kernels given by semi-infinite Fourier-inversion integrals with respect to $\lambda$. The same 32 point Gauss–Legendre, Gauss–Hermite and Gauss–Chebyshev quadratures are used to evaluate the integrals with respect to $\lambda$ or $\theta^*$. The only fundamental difference between the integrals in the expression for the side-layer variables in terms of $F$ and $G$, and the integrals in the two, coupled integral equations, is that each of the former semi-infinite integrals with respect to $\lambda$ includes either $\sin(\lambda Z)$ or $\cos(\lambda Z)$, which arise from the Fourier inversion for $Z \neq 0$.

## 4. Side-layer velocity profiles

Typical profiles of $V_r$ and $V_\theta$ are presented in figure 3. The values $\theta = 0.47$ and 1.00 rad correspond to Gauss–Chebyshev abscissas for $\theta_0 = 1.1071$ rad = arctan (2). Each profile of $V_r$ involves an overshoot region where $V_r > 1$. The excess volume flux in the overshoot cancels the deficiency in regions where $V_r < 1$, and the side-layer displacement thickness is zero everywhere.

The unexpected result is the very small magnitude of $V_\theta$ (and of $P$ and $J_r$). There does not appear to be any indication in the boundary-value problem (11, 14*a–c*, 15*a*, 16, 17, 18) that $V_\theta$ is small. However, $V_\theta$ still plays an important physical role, since it is necessary for the overshoot in $V_r$. If we replace the right-hand side of (11*b*) by zero, then the solution of the problem (11*b*, *c*, 14*b*, *c*, 15*a*, 17*b*, *c*) is $V_\theta = P = 0$. Then

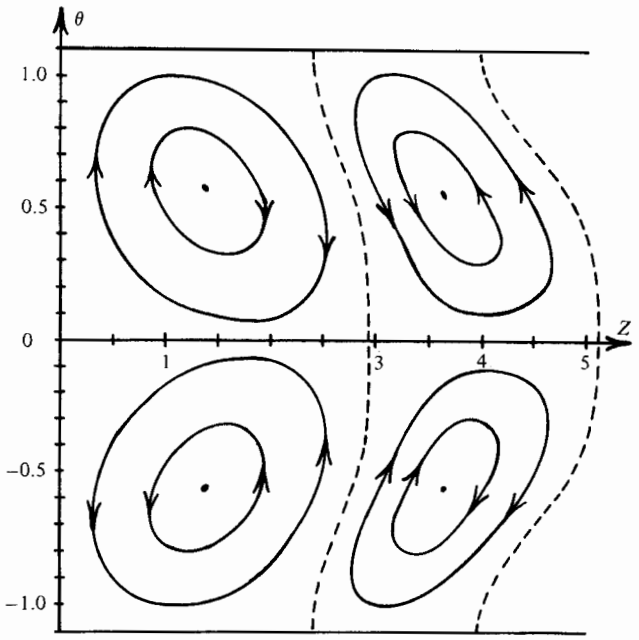


FIGURE 4. Sketch of principal vortices in $r$ = constant surfaces for the secondary flow in the side layers.

the right-hand side of (11$a$) is zero, and the problem (11$a$, 14$a$, $d$, 16, 17$a$) is precisely the side-layer problem solved by Hunt & Stewartson (1965) for fully developed flow in a constant-area rectangular duct with the same wall conductivities and with a uniform magnetic field. Their profiles of the axial velocity are monotonic and involve no overshoots. Therefore, their side-layer displacement thickness, $h'$ and the $O(M^{-\frac{1}{2}})$ core perturbation variables are not zero. Indeed, the present derivation of the boundary condition (18) and the proof of zero side-layer displacement thickness depend on the right-hand side of (11$b$).

Without the secondary flow associated with $V_\theta$, the side layer cannot match the core $V_r$, satisfy the no-slip condition (4$a$) at the side and have zero displacement thickness. The weak secondary flow provides the extra degree of freedom needed by $V_r$ to satisfy all three of these criteria. In figure 3 the dashed lines for $V_r$ and the dot–dashed lines for $V_\theta$ for the same $\theta$ and $\theta_0$ indicate that the regions of positive and negative $V_\theta$ for $\theta > 0$ correspond approximately with the regions of positive and negative $\partial V_r/\partial Z$ respectively.

The core flow (8) is purely radial, but the side-layer flow involves a weak secondary flow in $r$ = constant surfaces superimposed on the primary flow. The primary flow in the side layer consists of $V_r$ and that part of $V_z$ which is associated with the first right-hand term in (12$b$) and which is due physically to the fact that the actual side layers are spreading away from the sides as $r$ increases. The secondary flow consists of $V_\theta$ and the part of $V_z$ associated with the last term in (12$b$). There are four principal vortices in the secondary flow, as sketched in figure 4. Mathematically there is an infinite succession of pairs of vortices as we move away from the side, but their amplitudes decrease exponentially with $Z$ and are too small to be considered physically real or significant beyond the two pairs nearest the side.

Tabeling & Chabrerie (1981) found similar side-layer secondary flows in fully

developed flows in annular rectangular ducts with uniform magnetic fields. Their secondary flows are driven by an inertial force associated with the duct's curvature, while the present secondary flows are due to the gradient of the non-uniform magnetic field. Nevertheless, they also find an infinite succession of exponentially weakening vortices associated with an overshoot in the axial side-layer velocity profile.

We cannot compare side-layer velocity profiles for the same duct in the presence of uniform and non-uniform magnetic fields, since these profiles represent similarity solutions based on different scalings in these two cases. For example, in real variables, the side-layer transverse dimensions increase as $r$ and $r^{\frac{1}{2}}$ for polar non-uniform and uniform magnetic fields respectively, so that the same values of $Z$ in the two cases do not correspond to each other.

For a semi-infinite duct, $r_1 \leqslant r < \infty$, in a polar magnetic field, the present solution holds for a near region for $r = O(1)$. The assumptions $N \gg M \gg 1$ involved the characteristic quantities at $r = 1$, but the local $N$ and $M$ decrease as $r^{-2}$ and $r^{-1}$ respectively, so that our assumptions fail far downstream. We continue to use half the distance between the sides for $L$ because this is the dominant dimension far downstream. As we move downstream, the side layers spread across the duct and merge to become a viscous or viscous–inertial core, which ultimately evolves into a parabolic Poiseuille profile with decreasing magnitude or into a comparable velocity profile. The far downstream core could be studied by compressing the radial scale with $R = \delta r$, where $\delta$ depends on the relationship of the local $N$ and $M$, and the far downstream core at $R = 0$ would match the present solution as $r \to \infty$. For finite-length ducts, $r_1 \leqslant r \leqslant r_2$, the present solution requires that

$$N r_2^{-2} \gg M r_2^{-1} \gg M^{\frac{1}{2}} r_2^{-1} \gg 1,$$

where $N$ and $M$ are the constant parameters defined in §2, while the final condition ensures that the side layers are still thin at the exit.

## 5. Discussion

The physical reasons for the differences between the present flows and other three-dimensional MHD flows or fully developed flows are revealed by the consideration of certain characteristic surfaces for MHD flows. For a general three-dimensional magnetic field let $s$ by the distance measured along a magnetic field line and $B(s)$ be the local magnetic field strength at each point along this line. If each field line has two intersections with the electrically insulating or slightly conducting (thin-metal) walls confining the liquid metal, say at $s_1$ and $s_2$, then each magnetic field line has a value for a scalar quantity given by

$$K = \int_{s_1}^{s_2} B^{-1} \, \mathrm{d}s.$$

If $K$ has the same value for every magnetic field line, then there are no distinct characteristic surfaces, and the flow is 'free'. If $K$ varies, then a set of magnetic field lines with the same value of $K$ define a characteristic surface, and the flow is either 'guided' or 'blocked'. These terms are borrowed from geostrophic rotating flows, which are analogous to MHD flows with strong magnetic fields. However, the situation with MHD is somewhat more complex because both electric current and velocity are involved.

In a core region, the pressure must be constant on a characteristic surface, while the electric current must flow along it and must be parallel to the wall at the wall–field

intersection. The velocity perpendicular to a characteristic surface and the variation of the electric potential function along this surface are proportional to the electric current tangential to the surface. If there is an $O(1)$ current flowing along a surface, then there can be a proportional $O(1)$ velocity perpendicular to the surface and an $O(1)$ voltage variation along the surface (Holroyd 1980*a*). However, if an $O(1)$ current cannot flow along a characteristic surface, then there can be no $O(1)$ velocity perpendicular to the surface, and the flow must follow the characteristic surfaces (Holroyd & Walker 1978). These aspects of the characteristic surfaces lead to four different flow situations.

1. *Free flows with the same K for every magnetic field line.* For example, a uniform magnetic field perpendicular to a pair of parallel insulating or thin-metal walls gives a free flow, no matter what the geometry or electrical conductivity of the sides parallel to the field. In this case, the core flow is a first-order two-dimensional potential flow in planes perpendicular to the field; the sidewall boundary layers involve a monotonic tangential velocity profile for perfectly conducting sides; there is a second-order $O(M^{-\frac{1}{2}})$ potential core flow which compensates for the volume flux deficiency in the sides layers. Specifically, there is a jump in the $O(M^{-\frac{1}{2}})$ $\phi$ across the side layers which is proportional to the local volume flux deficiency, but the $O(M^{-\frac{1}{2}})$ core $\phi$, which satisfies a two-dimensional Laplace equation, can accommodate the variable boundary condition at the sides which results from the jump across the side layers. Fully developed flow is a special case of the free flows with infinite, parallel sides and with no axial variations (Walker *et al.* 1971).

2. *Guided flows with axial characteristic surfaces.* If the characteristic surfaces extend far upstream and downstream, then the fluid can flow along the duct by following the characteristic surfaces and with no $O(1)$ electric currents. The long surfaces also allow very slow migration of the flow across surfaces over long distances. This is the case for variable-area circular ducts in uniform or non-uniform magnetic fields and for circular pipes in non-uniform fields (Holroyd & Walker 1978).

3. *Blocked flows with transverse characteristic surfaces.* If the characteristic surfaces are essentially perpendicular to the flow direction and intersect insulating or thin-metal *sides*, then the sides block any $O(1)$ electric current and there can be no $O(1)$ velocity perpendicular to the surfaces, i.e. no $O(1)$ core velocity in the flow direction. In this case, the core is blocked, and the fluid here is essentially stagnant. The entire volume flux is carried by a large, $O(M^{\frac{1}{2}})$, axial velocity in the side layers. This is the case for insulating or thin-metal rectangular ducts with variable areas and uniform or non-uniform magnetic fields or with constant areas and variable fields (Walker *et al.* 1972).

4. *Guided flows with transverse characteristic surfaces.* If the sides in case 3 are replaced by perfect conductors, then these sides will accept any $O(1)$ electric current, so that there can now be an $O(1)$ core velocity perpendicular to the characteristic surfaces, and this core velocity can carry the volume flux down the duct. Unlike the free flow in case 1 with its relatively flexible potential core flow, this guided core flow is very restricted: the core axial velocity, transverse current and electric potential function are all determined, e.g. (8, 9). In particular, the jump in electric potential across the side layer is determined without solving the side-layer problem, and the side layer must accommodate this jump, while, for free flows, the jump in potential across the side layer is a result of the side-layer solution. In the present problem and others with parallel, perfectly conducting sides, the jump in potential is zero, so that the side layers must have zero displacement thickness. On the other hand, with diverging or converging sides, there is a jump in the $O(1)$ electric potential across the

side layers, which means that an $O(1)$ volume flux is carried by an $O(M^{\frac{1}{2}})$ velocity in these layers. Dependening on the divergences and the magnetic-field variations, these side jets may flow upstream or downstream (Walker *et al.* 1971). This case 4 is one case which does not occur in rotating flows. If a geostrophic surface intersects a solid wall parallel to the axis of rotation, then the flow is blocked. Here we can still have flow with 'blocked' surfaces, if the sides will accommodate the required electric current along the surfaces.

The transition between guided or blocked flows and free flows occurs when the variation of $K$ is $O(M^{-1})$. If the variations of $K$ are much less than $M^{-1}$, then the flows are essentially free; if the variations of $K$ are much greater than $M^{-1}$, then the flows are essentially guided or blocked.

The present problem falls into case 4, but there are still physically significant subcategories within this case. Variations of $K$ and the associated characteristic surfaces result from variable areas and/or variable magnetic fields. For the side layers, the distinction between free and guided or blocked flows is reflected in the coupling between the boundary-value problems governing $\phi$ and the velocity along the magnetic field lines $v_B$, i.e. $v_\theta$ here. For free flows, there is no coupling. The proof of zero displacement thickness given in §3 depends on this coupling, as represented by the right-hand side of (11 *b*). For free flows with no coupling, this proof does not apply, and, indeed, the side layers have non-zero displacement thicknesses.

A variable $K$ and the associated characteristic surfaces can be achieved with a uniform magnetic field by diverging or converging the top and bottom (Walker *et al.* 1971). In this case, the terms on the right-hand sides of (11 *a*, *b*) are replaced by zeros, but the boundary-value problems are coupled through the boundary conditions at the top and bottom. The proof of zero displacement thickness applies to this case too, even though the coupling is through the boundary conditions instead of the governing equations.

Variable-$K$ flows with characteristic surfaces can be grouped into three categories: (*a*) variable area with a uniform transverse magnetic field; (*b*) non-uniform magnetic field with variations of magnetic field strength $B$ between field lines, but not along field lines, i.e. $\mathrm{d}B/\mathrm{d}s = 0$; and (*c*) non-uniform magnetic field with variations of $B$ between and along field lines. For case (*b*) the field must be polar. Therefore the present analysis represents an extension from a uniform magnetic field (case *a*) to a non-uniform magnetic field, but with the effects of the variations of field strength along field lines suppressed by the restriction to a polar field (case *b*).

The present restriction to radial top and bottom was not necessary for the analysis. The present analysis and computer program apply equally well to a polar field with insulating top and bottom at $\theta = \pm\theta_0(r)$, including a constant-area duct with $\theta_0(r) = \arcsin(a/r)$, where $a$ is half the constant distance between the parallel top and bottom. Non-radial top and bottom would bring another parameter related to $\mathrm{d}\theta_0/\mathrm{d}r$ into the local side-layer solution. However, the radial top and bottom were specifically chosen to emphasize the effects of a variable magnetic field in a guided flow. We are interested in the effects of the coupling reflected by the right-hand sides of (11 *a*, *b*), which are present because of the variation of field strength between field lines.

With non-radial top and bottom, $v_\theta$ would have been driven by both these variable-field effects and the effects of the coupling through the boundary conditions at the top and bottom, e.g. $v_\theta = \pm v_r \mathrm{d}\theta_0/\mathrm{d}r$, at $\theta = \pm\theta_0$. For non-radial top and bottom, the effects of the two different couplings through the equations and the boundary conditions could not be separated; for radial top and bottom, only the coupling through the equations is present, so that its effects are revealed.

We have found two effects: one old and one new. First, $v_r$ has an overshoot, so that the displacement thickness of each side layer is everywhere zero. However, this is also true for variable-area ducts in uniform transverse magnetic fields. Secondly, even though the field lines are perpendicular to the top and bottom, there is still a velocity along the field lines, namely $v_\theta$, which reveals a secondary flow in the characteristic surfaces inside the side layers. There is no corresponding result for variable-area ducts in uniform fields, because, when the top and bottom are perpendicular to the field, the flow is free, and $v_B = 0$.

The extension to the case (*c*) with an unrestricted non-uniform magnetic field is needed to complete our understanding of MHD flows. However, it appears to be impracticable to extend the present method. With field variations along magnetic lines, the coupled ordinary differential equations obtained from the Fourier transforms of (11) would involve variable coefficients. Their analytical solution through variation of parameters or Green functions is theoretically straightforward, but practically impossible, because of the amount of algebra that would be involved. An approach with more numerics and less analysis has a greater promise of success with reasonable effort.

This research was supported by the U.S. National Science Foundation under Grant CPE-8108952. The authors are grateful to the referees, whose suggestions led to significant improvements in the presentation and interpretation of the present results.

## REFERENCES

HOLROYD, R. J. 1979 An experimental study of the effects of wall conductivity, non-uniform magnetic fields and variable-area ducts on liquid metal flows at high Hartmann number. Part 1. Ducts with non-conducting walls. *J. Fluid Mech.* **93**, 609–630.

HOLROYD, R. J. 1980*a* MHD flow in a rectangular duct with pairs of conducting and non-conducting walls in the presence of a non-uniform magnetic field. *J. Fluid Mech.* **96**, 335–353.

HOLROYD, R. J. 1980*b* An experimental study of the effects of wall conductivity, non-uniform magnetic fields and variable-area ducts on liquid metal flows at high Hartmann number. Part 2. Ducts with conducting walls. *J. Fluid Mech.* **96**, 355–374.

HOLROYD, R. J. & WALKER, J. S. 1978 A theoretical study of the effects of wall conductivity, non-uniform magnetic fields and variable-area ducts on liquid-metal flows at high Hartmann number. *J. Fluid Mech.* **84**, 471–495.

HUNT, J. C. R. & SHERCLIFF, J. A. 1971 Magnetohydrodynamics at high Hartmann number. *Ann. Rev. Fluid Mech.* **3**, 37–62.

HUNT, J. C. R. & STEWARTSON, K. 1965 Magnetohydrodynamic flow in rectangular ducts. Part 2. *J. Fluid Mech.* **23**, 563–581.

LUDFORD, G. S. S. & WALKER, J. S. 1976 On establishing fully developed duct flow in strong magnetic fields. In *MHD-Flows and Turbulence* (ed. H. Branover), pp. 7–15. Wiley: Israel Universities Press.

LUDFORD, G. S. S. & WALKER, J. S. 1980 Current status of MHD duct flow. In *MHD-Flows and Turbulence II* (ed. H. Branover & A. Yakhot), pp. 83–95. Israel Universities Press.

PETRYKOWSKI, J. C. 1981 A three-dimensional magnetohydrodynamic duct flow in a non-uniform magnetic field. Ph.D. dissertation, University of Illinois at Urbana-Champaign.

TABELING, P. & CHABRERIE, J. P. 1981 Magnetohydrodynamic secondary flows at high Hartmann numbers. *J. Fluid Mech.* **103**, 225–239.

WALKER, J. S. 1980 Large interaction parameter magnetohydrodynamics and applications in fusion reactor technology. In *Fluid Mechanics and Energy Conversion, Proc. SIMS Conf.*, pp. 215–229. SIAM.

WALKER, J. S. 1981 Magnetohydrodynamic flows in rectangular ducts with thin conducting walls. Part 1. Constant-area and variable-area ducts with strong uniform magnetic fields. *J. Méc.* **20**, 79–112.

WALKER, J. S. & LUDFORD, G. S. S. 1975 Duct flow in strong magnetic fields. *Recent Adv. Engng Sci.* **6**, 329–335.

WALKER, J. S., LUDFORD, G. S. S. & HUNT, J. C. R. 1971 Three-dimensional MHD duct flows with strong transverse magnetic fields. Part 2. Variable-area rectangular ducts with conducting sides. *J. Fluid Mech.* **46**, 657–684.

WALKER, J. S., LUDFORD, G. S. S. & HUNT, J. C. R. 1972 Three-dimensional MHD duct flows with strong transverse magnetic fields. Part 3. Variable-area rectangular ducts with insulating walls. *J. Fluid Mech.* **56**, 121–141.